Pierret, C.; Maunoury, L.; Monnet, I.; Bouffard, S.; Benyagoub, A.; Grygiel, C.; Busardo, D.; Muller, D.; Hoeche, D.:

Friction and wear properties modification of Ti–6Al–4V alloy surfaces by implantation of multi-charged carbon ions

In: Wear (2014) Elsevier

DOI: 10.1016/j.wear.2014.07.001

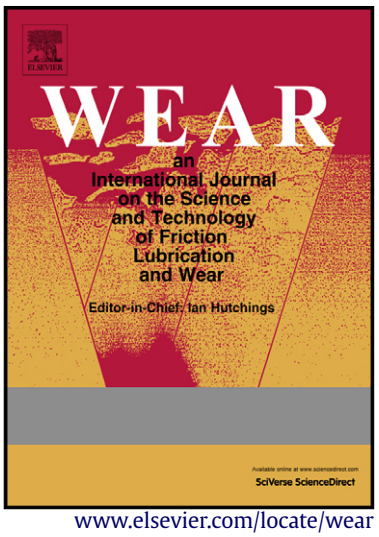

www.elsevier.com/locate/wear

Friction and wear properties modification of ti-6Al-4V alloy surfaces by implantation of multi-charged carbon ions

C. Pierret, L. Maunoury, I. Monnet, S. Bouffard, A. Benyagoub, C. Grygiel, D. Busardo, D. Muller, D. Hoche

PII: S0043-1648(14)00215-4
DOI: http://dx.doi.org/10.1016/j.wear.2014.07.001
Reference: WEA101059

To appear in: *Wear*

Received date: 23 January 2014
Revised date: 2 July 2014
Accepted date: 2 July 2014

Cite this article as: C. Pierret, L. Maunoury, I. Monnet, S. Bouffard, A. Benyagoub, C. Grygiel, D. Busardo, D. Muller, D. Hoche, Friction and wear properties modification of ti-6Al-4V alloy surfaces by implantation of multi-charged carbon ions, *Wear,* http://dx.doi.org/10.1016/j.wear.2014.07.001

Friction and wear properties modification of Ti-6Al-4V alloy surfaces by implantation of multi-charged carbon ions

C. Pierret[a,b], L. Maunoury[c], I. Monnet[a], S.Bouffard[a], A. Benyagoub[a], C. Grygiel[a], D. Busardo[b], D. Muller[d], D. Höche[e*1]

a *Centre de Recherche sur les Ions, les Matériaux et la Photonique, CEA-CNRS-ENSICAEN-Université de Caen Basse-Normandie, 6 bd du Maréchal Juin, F-14050*
b *Quertech Ingénierie, 9 rue de la Girafe, 14000, France*
c *GANIL, CEA/DSM CNRS/IN2P3, Boulevard Henri Becquerel, B.P. 55027, F-14076 Caen cedex 05, France*
d InESS, Université de Strasbourg and CNRS, 23 rue du Loess, B.P. 20, 67037 Strasbourg cedex 2, France
e Helmholtz-Zentrum Geesthacht Zentrum für Material- und Küstenforschung GmbH, Institute of Materials Research, Max-Planck-Straße 1, D-21502 Geesthacht, Germany

Abstract

Carbon implantation into titanium is known to enhance some of its surface properties like wear behavior, mechanical hardness or the friction coefficient. Therefore the method is a candidate to be applied as a powerful surface engineering tool for titanium alloys. Recently, there has been developed a new implantation technique, which based on a compact particle accelerator device being easy to handle. The device allows simultaneous multi-charged ion-implantation (from C^{+} up to C^{4+}) in order to get a plateau like implantation profile based on the energetic distribution. The aim of this study is to investigate microstructural modifications of the near surface region of Ti-6Al-4V due to this processing technology and to enhance the surface performance. Nanoindentation and tribological measurements revealed a threshold of critical C - contents where friction coefficient and wear are significantly reduced. Furthermore, these enhancements have been correlated to the presence of additional graphitic carbon.

Keywords: Ion Implantation, Titanium Alloys, Carbiding, Carbon Depth Profile

1. Introduction

Titanium and titanium alloys are used in numerous and various fields of application due to their interesting properties like: high strength, low density, excellent corrosion resistance, efficient biocompatibility etc. It can be used to design engine parts in aeronautics, prostheses or implants in

[1] Corresponding author: Dr. Daniel Höche: Helmholtz-Zentrum Geesthacht, Institute for Materials Research, Corrosion & Surface Technology, Max-Planck Str.1, DE-21502 Geesthacht, ☎ ++49-(0)4152/87-1914, ✉ daniel.hoeche@hzg.de

biomedicine [1, 2]. However, their main weakness is a mediocre friction and wear resistance. For specific applications in biomedical or aeronautic field for example, the surface of titanium alloys must be treated or strengthened in order to get a smaller friction coefficient, to delay crack ignitions or to reduce wear particle releases. Beside classical coating technologies [3-5], ion implantation is an appropriate surface treatment process for that purpose [6]. The method is already known to enhance surface properties of metals [7, 8] and especially of titanium alloys [9-11] but was used with difficulty for industrial applications due to the complexity and the high cost of this process.

An original ion implantation method was developed by Quertech Ingénierie [12]. This new process (trademark Hardion+) is based on the operation of a compact ECR (Electron Cyclotron Resonance [13]) ion source to provide ion beams allowing simultaneously implantation of multi-charged multi-energized ions into materials and compounds. Multi-charged nitrogen ion implantation was already applied to titanium alloys in previous works [14, 15]. A compact mass spectrometer was developed specially to produce multi-charged carbon beams (from 1+ up to 4+ meaning energy from tens of keV up to hundreds of keV) at low cost and without complex optic ion beam systems. Based on this unique device target oriented surface processing of Ti-6Al-4V by carbon ion bombardment was carried out. This study shows the achieved result based on investigations of microstructural changes within the near surface region and points out the aspects of surface property modifications due to simultaneous multi-charged carbon implantation.

2. Technical Setup and Micro mass-spectrometer device

In order to generate carbon ion beams with an ECR ion source [16], it is necessary to inject carbon atoms under gaseous state, to ionize them as multi-charged state ions and further to separate the arising beams from the secondary, so called “pollutant” beams (hydrogen - oxygen – nitrogen). The Quertech micro-implanter is a very compact device and provides an ion beam with a high intensity ($I > 2$ mA) deducing a reduced treatment time. The neutral carbon atoms are obtained by using gaseous compounds based on bonded carbon (hydrocarbon, carbon dioxide, etc.). Using the C_xH_y family enables high ionization efficiency and at least high beam intensities (from several hundred nA to a few mA). Sadly, this induces high so called hydrogen pollution. Due to the tiny space available in

the treatment chamber, a micro mass-spectrometer has been specifically designed. The micro mass-spectrometer keeps the carbon multi-charged beams together in close trajectories and, separates those beams from the intense hydrogen mono-charged "pollutant" beam. The magnetic structure of the device was designed with RADIA [17] and the ion trajectories were calculated by SIMION 3D and CPO 3D [18-20]. The spatial separation between the hydrogen beam and the carbon beams is in the order of several centimeters. The working principle of the micro mass-spectrometer is shown in the following Figure 1.

Figure 1: Schemata of a micro mass-spectrometer and its working principles for controlling and separating hydrogen and carbon ion trajectories.

After measuring the carbon ion beam intensity by a faraday cup and as well as determining the beam profile, ion trajectories have been calculated to layout the processing. It has been shown that the beam composes of charge states ranging from 1^+ up to 4^+ with an average charge state of 1.45^+. Figure 2 shows a chart, of a typical calculation by SRIM at 100 keV incident beam energy, of carbon implantation into Ti-6Al-AV and the arising carbon atomic concentration depth profile within the upper surface region of the Ti-6Al-4V alloy for Hardion$^+$ technology. The profile in figure 2 b) shows up a tail due to the higher charge states of the carbon which is the main difference compared to a profile with a single charge state (shown as a) case).

Figure 2: a) SRIM 2008 simulation of $C^{1.45+}$ of 100 keV into Ti-6Al-4V b) SRIM 2008 based calculation of multi-ion carbon depth distribution into Ti-6Al-4V with an average state of 1.45

In the following sections, the treated samples are labeled with number 0 to 5 corresponding to increasing fluencies described in table 1. They are sorted according to their maximum carbon concentration (all concentrations in this article are in at.%) in order to have a better comparison with mono-charged ion implantation done in previous work. Obviously the carbon concentration is directly correlated to ion fluence [21, 22]. A more detailed description can be found in a recent work [23].

Table 1: Maximum carbon concentrations derived from RBS measurements (+/- 3%) [22] and SRIM 2008 calculation as well as the derived average implantation depth.

Table 1 clearly shows that SRIM calculations are very close to the values being found during RBS measurement. Thus, even if sample 2 has not been measured by RBS (for technical reasons), it can be assumed that the carbon maximum concentration value from the calculation can be used.

The amount of specimens was limited due to the extensive time consumption of necessary pretreatments, blind tests and analyses, and the fixed ability time of the micro-implantor device for final treatments at optimized setups. Thus, the relative error is high for statistical reasons.

3. Experiments

Ti-6Al-4V samples (20 mm x 20 mm) were cut from commercial sheets, mechanically grinded up to 4000 grit abrasive papers, polished with silicon oxide solution, and then cleaned with acetone and ethanol. Ion implantation was carried out with the micro-implanter coupled to the micro-mass-spectrometer described in the previous section. The pressure was 3.10^{-6} mbar inside the vacuum chamber, the used fluence ranged from several 10^{17} to a few 10^{18} ions.cm^{-2} and the ion beam current was measured to be 1 mA. During the implantation process the energy was set to several tens of keV per charge and the ion implantation fluence was chosen in order to have high carbon maximum concentration (table 1).

Rutherford Back Scattering method was employed to measure the carbon depth profile and the carbon concentration at the titanium pieces. The required 2 MeV He^+ beam is delivered by the 4 MV Van De Graaff accelerator [24] at InESS – Strasbourg and the scattering angle was fixed at 160°. Phase identification has been performed applying Raman spectrometry (at a wave length of 532.1 nm) with a beam power varied from 4 to 20 mW during the measurements. Grazing incidence X-ray diffraction was performed to study the crystallographic structure of the implanted Ti alloys by using a D8 Discover BRUKER diffractometer with a Cu-K_α anticathode ($\lambda_{K\alpha1}$ = 0.154056nm, $\lambda_{K\alpha2}$ = 0.154442nm) [25]. X-ray diffraction patterns were recorded in θ-θ geometry by using a grazing incident angle of 1° in a range between 20–80°, utilizing a step size of 0.031°. The penetration depth of the X-ray beam at

1° incident angle corresponds to an information depth of approximately 450nm. X-ray induced photoelectron spectroscopy (XPS) experiments were carried out on a Kratos Axis Ultra DLD attached with a 15 kV X-ray gun using monochromatic Al-K_α radiation applying the setup used in reference [15]. The analyzed area size was 700×300 µm and the pass energy was set to 40 eV at the regions measurements. Due to physical limits the information depth is limited to approx. 5 nm. Additionally, argon ions (4 keV) have been used to etch the samples for different times in order to obtain depth profiles.

Surface mechanical properties were studied employing nanoindentation with a CSM NHT instrument equipped with a diamond Berkovich tip. For statistical reasons, eighteen indentations were made perpendicularly to the sample surface using an oscillating mode that finally permits hardness-depth profile plots. Ball-on-disk tribological tests were performed several times with a CSM tribometer to evaluate the mean friction coefficients and to investigate the wear resistance of the processed surfaces. The friction coefficient was monitored during sample surface sliding in relation to an alumina ball (6 mm diameter) in ambient atmosphere without using a lubricant. The applied loads and the sliding velocity being used were chosen to be 0.25 N, 0.5 N, and 0.01 $m.s^{-1}$. These parameters offer comparable data to the one being used by D.M. Gordin et al. for testing surface modifications for biomedical applications induced by nitrogen multi-charged ion implantation [14, 15].

The to be expected shear stress and the depth of maximum shear stress for 0.5 N load can be calculated according Hertz theory based contact model [26, 27]. Assuming an ideal Ti-C / alumina configuration at 0.5 N load the maximum acting shear stress will be around 0.25 GPa within a depth range of 5-10 µm.

RBS spectra were used to evaluate the concentration and the implantation depth profile of carbon atoms in the implanted samples. For that purpose, the spectra were analyzed by SAM - "Simulation for Analysis of Materials" software developed by InESS laboratory as a part of the VRBS [28] package.

The average ion implantation depth varied from 110 nm to 190 nm for the test samples. Thereby, the maximum carbon atomic concentration varied from 30% to 90%. That measured concentrations and those calculated by SRIM 2008 [29] are comparable as it can be seen in table 1.

Obviously, the multi-charged ion implantation technology can be applied and controlled by taking care to the standard scattering theory.

3.1. Mechanical properties

Nanoindentation measurements were performed onto the entire surface. Mean hardness versus tip penetration depth profiles plot of treated and non-treated samples has been shown in figure 3. All samples reveal a hardness enhancement at approx. 300 nm in depth after carbon irradiation, with a maximum hardness value reached around 100-150 nm in depth, which is followed by a smooth decrease. The maximum, universal hardness reaches values of 7.5 GPa (sample 1) up to 9.25 GPa (sample 5). For the non-implanted sample 0, such an increase of the hardness has also been observed, due to the mechanical polishing, but in a pronounced way. The achieved improvements mainly based on TiC phase formation, which will be verified in the next sections.

Figure 3: Universal hardness depth profiles for different processing situations according to table 1.

In order to be able to compare results to other works and publications, we defined a relative hardness gain which is the ratio between maximum hardness and initial hardness being independent from absolute values. Figure 4 indicates the relative hardness gain versus carbon maximum concentration found in this study and compares it, with those found by others authors [30-33]. It becomes clear that simultaneous multi-charged ion-implantation offers a comparable performance of hardness improvement compared to mono-energetic carbon implantation processes. Wenzel et al. performed carbon implantation on Ti and not in Ti-6Al-4V. Additionally, heating was carried out during the ion irradiation leading to enhanced carbon transport and increased carbide formation. This might explain the higher values being found. Nevertheless, some advantages occur by applying this setup. One is the reduction of the treatment duration and another one the ease of use of the micro implanter. Both are important arguments to facilitate its use in industrial applications.

Figure 4: Relative hardness gain versus carbon maximum concentration for the measurements (•) compared to previous research studies [30-33].

Figure 5 shows the dependency of the friction coefficient to the cycle number for a load of 0.25 N. Friction coefficients of non-treated samples increase rapidly to high values (0,6 - 0,7) even at the beginning of the tests. The non-treated samples showed a poor friction behavior, characterized by high and unstable friction coefficients, which extensively fluctuate during the sliding tests. The friction coefficients of the implanted samples are lower than the coefficients of the non-implanted one. For sample 1 and 2, the friction coefficient is lower than for the sample 0 (non-implanted) and they reach the non-implanted sample friction coefficient after 150 cycles. For sample 3, 4 and 5 the behavior is quite different. The number of cycle where the friction coefficient increases progressively varies from 2900 cycles for sample 3 to 6300 cycles for sample 5. Thus one can state: as more carbon has been implanted, as more the friction coefficient gets improved up to saturation, which has been verified for a large number of cycles beyond 1000.

Figure 5: Mean friction coefficient measured by the Ball-on-disk test (average curves) as a function of the number of cycles for a load of 0.25 N.

To validate this result, additional tests were performed applying another load of 0.5 N. Figure 6 shows the cycle number for the ball-on-disk test, up to the point where the friction coefficient increases to achieve the initial value. For the present case this corresponds to a value of 0.55. Similar results have been observed. Especially, significant improvements of the mechanical properties for the high carbon amount samples 3 to 5 have been shown. The experiments revealed that the carbon dose being implanted strongly correlates to the achieved improvement and at least governs the engineering and application ability. The observed behavior implies a kind of carbon concentration threshold for significant improvements around 60%. There are two contenders for this aspect. First one is the required formation of titanium carbide as a wear protecting functional coating. The second one, and even more interesting, is the C-C bond based graphitic top layer, which provides wear protection also by acting as a kind of lubricant.

Figure 6: Cycle number before friction coefficient increases, applying loads of 0.25 N and 0.5 N for different achieved surface states after implantation processing.

After the tribological tests, the ball was not intact due to similar Young's modules of TiC and alumina. The surface of the testing devices had been covered by black compounds, which is intended to be carbon and a mixture of intermetallic compounds and oxides (according to comparable studies of Qu et al. [34]). Thus, the relative position at the ball surface was changed between two tests. Figure 7 shows wear tracks after 200 cycles of friction tests at a load of 0.5 N. Sample 1 - 2 have large wear tracks compared to the untreated one. Surprisingly, samples 3 and 4 have wear tracks reduced by a factor two in width. Furthermore, wear is reduced by a factor of five for the sample 5 (Figure 8). Hence, one can state that wear is augmented for low carbon fluence during the implantation process, but it is reduced for applied fluences equal or superior to the one being used during processing of sample 3. The summary of the last test results, especially that being carried out at sample 1 and 2, reveal a disappointing wear performance. At sample 3 the situation changes and a significant improvement was achieved.

It is difficult to compare friction coefficients from the tribological tests with that being measured by other groups. Indeed for being suitable to compare, tests must be done at the same conditions, which means to answer questions like: Do they use lubricants (here, they did not have been used)? Which force was applied? What type of ball was used (radius of the ball)?, etc. Nevertheless, the results exhibit a quality which supports the results of e.g. Wenzel et.al [33].

Figure 7: Optical micrographs of the surfaces, the wear tracks and measured track widths after 200 cycles with an applied load of 0.5 N.

Figure 8: Measured track widths after 200 cycles with an applied load of 0.5 N.

In context to the previous explained hardness improvement measured for all the samples (even for the lowest dose implanted one), the friction behavior is different. An improvement appears after a

certain threshold dose, which corresponds to critical carbon contents between 44% and 67% as indicated in figure 8. The observed property jump is expected to be related one the one hand to more efficient TiC formation at higher concentration, and on the other to carbon saturation respectively graphite formation dealing with lubricity. To gain an improved accuracy, further studies are required. In this manner wear volume fraction measurements or deep wear chemistry analysis might offer deeper understanding towards an optimized processing layout.

3.2 *Structural evolution*

X-ray diffraction patterns for samples 0, 2 and 4 are presented in figure 9. Three new peaks are observed after implantation beside the α-Ti pattern. These reflections are contributed to the face-centered cubic TiC phase with respectively the (*111*) reflection at 35.8°, (*200*) at 41.7° and (*220*) at 60.5° [10]. Any reflections are observed corresponding to the hexagonal graphite phase. These measurements highlight the formation of a single TiC phase for the carbon implanted samples.

Figure 9: GIXRD diffraction patterns of non-implanted T-6Al-4V (sample 0) and carbon implanted Ti-6Al-4V (samples 2 and 4).

Raman spectra are shown in Figure 10. For samples 0, 1 and 2, no peak signals have been detected. For the other samples being investigated two identical peaks are detected with different relative intensities. One, called D peak corresponds to amorphous carbon (1350 cm^{-1}) and the other one (G peak) is contributed to graphitic carbon (1550 cm^{-1}) [35]. These C-C bonds are only present for a certain carbon concentration (sample 3 to 5) and an indicator for significant surface modifications. The peak intensities increase with the fluence, which is a crucial hint on the growing crystallinity.

Figure 10: Raman spectra for all test samples according table 1 showing the crystallinity state of the different surface and implantation conditions.

XPS analysis was performed only for the highest dose implanted sample (sample 5) and is shown in figure 11. After a sputtering time of 1680 seconds using Ar^+ ions at 4 keV, the depth being analyzed

was about 520 nm+/- 40 nm. Two peaks appear clearly at the energy of 281.9 eV and 284.6 eV. They can be credited to C-C and Ti-C bonds respectively [21]. The C-C bonds are measured from the very surface down to a depth of approx. 200 nm whereas Ti-C bonds are identified from 180 nm to 300 nm depth. Similar results were found by Viviente & Garcia et al. [22, 30]. It means that a two layer system exists where the C-C layer (mainly graphite) is coated onto the Ti-C layer. The effect is contributed to saturation and to modified and shortened ion trajectories in the presence of e.g. Ti-C. Ti-O_2 bonds are also detected on the top of the surface but not deeper in the treated samples. That film is contributed to an oxidation of the first atomic layers of the alloy.

3.3. Discussion

The hardness increase can be related to the formation of TiC as shown by XRD. This phase is well known for its high hardness value [36, 37]. Complementary, the hardness augmentation might also be partially attributed to effects based on the lattice distortion, the dislocation hardening, and the residual compressive stress formed by implantation [31-33, 38].

Figure 11: XPS depth profiling of the C 1s (left) and Ti 2p (right) excitation for sample 5.

The tribological properties (friction coefficient and wear) seem to be not only associated to the carbiding effect but also to the C-C bonds. Indeed when these bonds are not detected the friction coefficient has been poorly improved and the wear performance was high, but tribological performance significantly increases as soon as C-C bonds are available. This effect is amplified when they are located close to respectively on the surface of the alloy. This aspect is contributed a kind of lubricant action which is well known for graphite.

In order to verify this assumption more tribological and spectrometric tests were performed. On all samples, two additional tribological measurements were performed. The first one was stopped after 200 cycles and the second one just after the friction coefficient reaches the value of the non-implanted (0,6). Figure 11 provides the Raman spectra for the different test conditions of sample 5 compared to sample 0. After 200 cycles, the C-C bond quantity has diminished for both cases. Succeeding the second test, C-C bonds do not have been detected anymore. The same result was

initially found on sample 4, but after 200 cycles, the C-C bond quantity decrease more than being observed for sample 5. Furthermore, the measurements show that sample 5 has better tribological performances in the previous state than sample 4. The explained effect is related to the C-C bonds quantity which is decreasing faster for sample 4 than for sample 5 (after 200 cycles). Considering all the aspects allows the conclusion that tribological performance is mainly contributed to C-C bonds and graphite formation. This explanation is also in agreement with the performance being measured for sample 1 and 2, where C-C bonds and a two layer system are missing.

Figure 12: Raman spectra of sample 5 for: (a) just after carbon implantation, (b) after a 200 cycles tribology test, (c) after the friction coefficient reaches the value of the non-implanted: 0.6; and (d) for a non-implanted sample (according sample 0)

Additional TEM investigations are suggested to continue the progress in wear and friction control by the multi-ion implantation process. Complementary surface characterization on the micro scale might reveal the best ratio of amounts of Ti-C / C-C bonds in the future. Common suggestions have been published and forwarded also by Shum et al. [11] in 2012.

4. Conclusion

Carbon implantation led to microstructural changes and mechanical properties modifications of Ti-6Al-4V. The formation of TiC compounds was demonstrated by XRD analyses explaining partially the hardness improvement which is increased in the first 300 nm. The depth profile shape is determined by the interactions of the two layer system Ti-C/C-C and the bulk material. Formation of C-C bonds were shown by Raman spectrometry and XPS analyses. The C-C bonds do not appear for low carbon concentration (<44% of carbon concentration) and they are positioned on top of the TiC layer on the entire surface. The process advantageously modifies tribological properties. It reduces friction coefficient even at a large number of cycles and shows a wear track width reduction up to 80%. Tribological enhancements behave to have a threshold (between 44% and 65% of carbon concentration) within the implantation fluence range (process control parameter) where tribological properties are improved in an accelerating way. This enhancement in sliding performance is mainly

due to the presence of graphitic carbon working as friction reducer respectively as lubricant. On the one hand, more measurement should be carried out in order to precise the measured value of this threshold. Finally, treated samples with carbon maximum concentration over 80% should be explored as to know whether surface properties are still enhanced.

References

[1] X.Y. Liu, P.K. Chu, C.X. Ding, Surface modification of titanium, titanium alloys, and related materials for biomedical applications, Mat Sci Eng R, 47 (2004) 49-121.

[2] P. Sioshansi, R.W. Oliver, F.D. Matthews, Wear improvement of surgical titanium alloys by ion implantation, Journal of Vacuum Science & Technology A, 3 (1985) 2670-2674.

[3] A. Shanaghi, A.R.S. Rouhaghdam, S. Ahangarani, P.K. Chu, T.S. Farahani, Effects of duty cycle on microstructure and corrosion behavior of TiC coatings prepared by DC pulsed plasma CVD, Appl Surf Sci, 258 (2012) 3051-3057.

[4] D. Höche, P. Schaaf, Laser nitriding: investigations on the model system TiN. A review, Heat Mass Transfer, 47 (2011) 519-540.

[5] W. Schintlmeister, O. Pacher, K. Pfaffinger, T. Raine, Structure and strength effects in CVD titanium carbide and titanium nitride coatings, Journal of The Electrochemical Society, 123 (1976) 924-929.

[6] N.E.W. Hartley, Ion implantation and surface modification in tribology, Wear, 34 (1975) 427-438.

[7] G. Dearnaley, Ion-Beam Modification of Metals, Nucl Instrum Meth B, 50 (1990) 358-367.

[8] D. Höche, C. Blawert, M. Cavellier, D. Busardo, T. Gloriant, Magnesium nitride phase formation by means of ion beam implantation technique, Appl Surf Sci, 257 (2011) 5626-5633.

[9] M. Guemmaz, A. Mosser, L. Boudoukha, J.J. Grob, D. Raiser, J.C. Sens, Ion beam synthesis of non-stoichiometric titanium carbide: Composition structure and nanoindentation studies, Nucl Instrum Meth B, 111 (1996) 263-270.

[10] B. Rauschenbach, Mechanical-Properties of Nitrogen Ion-Implanted Ti-6al-4v Alloy, Surf Coat Tech, 66 (1994) 279-282.

[11] P.W. Shum, Y.F. Xu, Z.F. Zhou, W.L. Cheng, K.Y. Li, Study of TiAlSiN coatings post-treated with N and C+N ion implantations. Part 2: The tribological analysis, Wear, 274–275 (2012) 274-280.

[12] D. Busardo, Method for treating a metal element with ion beam, in: Q. Ingénierie (Ed.), France, 2009.

[13] R. Geller, Electron cyclotron resonance ion sources and ECR plasmas, Taylor & Francis, 1996.

[14] D.M. Gordin, D. Busardo, A. Cimpean, C. Vasilescu, D. Höche, S.I. Drob, V. Mitran, M. Cornen, T. Gloriant, Design of a nitrogen-implanted titanium-based superelastic alloy with optimized properties for biomedical applications, Mat Sci Eng C-Mater, 33 (2013) 4173-4182.

[15] D.M. Gordin, T. Gloriant, V. Chane-Pane, D. Busardo, V. Mitran, D. Höche, C. Vasilescu, S.I. Drob, A. Cimpean, Surface characterization and biocompatibility of titanium alloys implanted with nitrogen by Hardion plus technology, J Mater Sci-Mater M, 23 (2012) 2953-2966.

[16] M. Muramatsu, A. Kitagawa, A review of ion sources for medical accelerators (invited), Rev Sci Instrum, 83 (2012).

[17] P. Elleaume, O. Chubar, J. Chavanne, Computing 3D magnetic fields from insertion devices, Particle Accelerator Conference, IEEE, Vancouver, 1997, pp. 3509-3511.

[18] M.L. Korwin-Pawlowski, K. Amiz, H. Elsayed-Ali, Modeling of a multicharged ion beam line using SIMION, Photonics North, International Society for Optics and Photonics, Quebec, 2009, pp. 73862B.

[19] H. Lai, T.R. McJunkin, C.J. Miller, J.R. Scott, J.R. Almirall, The predictive power of SIMION/SDS simulation software for modeling ion mobility spectrometry instruments, International Journal of Mass Spectrometry, 276 (2008) 1-8.

[20] F. Read, N. Bowring, The BEM Programs of CPO Ltd, pp. 25.

[21] J.L. Viviente, A. Garcia, F. Alonso, I. Braceras, J.I. Onate, X-ray photoelectron spectroscopy characterization of high dose carbon-implanted steel and titanium alloys, Appl Surf Sci, 144-45 (1999) 249-254.

[22] J.L. Viviente, A. Garcia, A. Loinaz, F. Alonso, J.I. Onate, Carbon layers formed on steel and Ti alloys after ion implantation of C+ at very high doses, Vacuum, 52 (1999) 141-146.

[23] C. Pierret, Mechanical and tribological behaviour of Ti-6Al-4V alloy after multicharged carbon and oxygen ion implantation. Carbon ion beam development, Université de Caen Caen, 2011.

[24] G. Amsel, J. Nadai, E. d'Artemare, D. David, E. Girard, J. Moulin, Microanalysis by the direct observation of nuclear reactions using a 2 MeV Van de Graaff, Nuclear Instruments and Methods, 92 (1971) 481-498.

[25] C. Grygiel, H. Lebius, S. Bouffard, A. Quentin, J.M. Ramillon, T. Madi, S. Guillous, T. Been, P. Guinement, D. Lelievre, I. Monnet, Online in situ x-ray diffraction setup for structural modification studies during swift heavy ion irradiation, Rev Sci Instrum, 83 (2012).

[26] R.L. Jackson, J.L. Streator, A multi-scale model for contact between rough surfaces, Wear, 261 (2006) 1337-1347.

[27] P. Põdra, S. Andersson, Simulating sliding wear with finite element method, Tribology International, 32 (1999) 71-81.

[28] J. Stoquert, F. Pêcheux, Y. Hervé, H. Marchal, R. Stuck, P. Siffert, VRBS: A virtual RBS simulation tool for ion beam analysis, Nuclear Instruments and Methods in Physics Research Section B: Beam Interactions with Materials and Atoms, 136 (1998) 1152-1156.

[29] J.F. Ziegler, J.P. Biersack, SRIM-2008, Stopping Power and Range of Ions in Matter, Organisation for Economic Co-Operation and Development, Nuclear Energy Agency-OECD/NEA, Le Seine Saint-Germain, 12 boulevard des Iles, F-92130 Issy-les-Moulineaux (France), 2008.

[30] A. Garcia, J.L. Viviente, F. Alonso, A. Loinaz, J.I. Onate, Growth of carbon layers on Ti-6Al-4V alloy by very high dose carbon implantation, Surf Coat Tech, 97 (1997) 499-503.

[31] D. Krupa, E. Jezierska, J. Baszkiewicz, T. Wierzchon, A. Barcz, G. Gawlik, J. Jagielski, J.W. Sobczak, A. Bilinski, B. Larisch, Effect of carbon ion implantation on the structure and corrosion resistance of OT-4-0 titanium alloy, Surf Coat Tech, 114 (1999) 250-259.

[32] J.I. Onate, F. Alonso, A. Garcia, Improvement of tribological properties by ion implantation, Thin Solid Films, 317 (1998) 471-476.

[33] A. Wenzel, C. Hammerl, A. Koniger, B. Rauschenbach, Formation of titanium carbide by high-fluence carbon ion implantation, Nucl Instrum Meth B, 129 (1997) 369-376.

[34] J. Qu, P.J. Blau, T.R. Watkins, O.B. Cavin, N.S. Kulkarni, Friction and wear of titanium alloys sliding against metal, polymer, and ceramic counterfaces, Wear, 258 (2005) 1348-1356.

[35] J.C. Sanchez-Lopez, D. Martinez-Martinez, C. Lopez-Cartes, A. Fernandez, Tribological behaviour of titanium carbide/amorphous carbon nanocomposite coatings: From macro to the micro-scale, Surf Coat Tech, 202 (2008) 4011-4018.

[36] Y. Kumashiro, A. Itoh, T. Kinoshita, M. Sobajima, The micro-Vickers hardness of TiC single crystals up to 1500 C, Journal of Materials Science, 12 (1977) 595-601.

[37] E. Hummer, A. Perry, Adhesion and hardness of ion-plated TiC and TiN coatings, Thin Solid Films, 101 (1983) 243-251.

[38] D. Krupa, J. Baszkiewicz, E. Jezierska, J. Kozubowski, A. Barcz, Effect of nitrogen, carbon and oxygen ion implantation on the structure and corrosion resistance of OT-4-0 titanium alloy, Nukleonika, 44 (1999) 207-216.

Tables

Sample number	Carbon maximum concentration (%)		Average implantation depth (nm)
	SRIM 2008 Calculation	RBS measurements	
0	Non implanted		
1	28	30	110
2	44	Not measured	Not measured
3	65	67	130
4	76	83	150
5	82	90	190

Table 1: Maximum carbon concentrations derived from RBS measurements (+/- 3%) [22] and SRIM 2008 calculation as well as the derived average implantation depth.

Captions

Table 1: Maximum carbon concentrations derived from RBS measurements (+/- 3%) [22] and SRIM 2008 calculation, as well as the derived average implantation depth.

Figure 1: Schemata of a micro mass-spectrometer and its working principles for controlling and separating hydrogen and carbon ion trajectories.

Figure 2: a) SRIM 2008 simulation of $C^{1.45+}$ of 100 keV into Ti-6Al-4V b) SRIM 2008 based calculation of multi-ion carbon depth distribution into Ti-6Al-4V with an average state of 1.45

Figure 3: Universal hardness depth profiles for different processing situations according to table 1.

Figure 4: Relative hardness gain versus carbon maximum concentration for the measurements (•) compared to previous research studies [30-33].

Figure 5: Mean friction coefficient measured by the Ball-on-disk test (average curves) as a function of the number of cycles for a load of 0.25 N.

Figure 6: Cycle number before friction coefficient increases, applying loads of 0.25 N and 0.5 N for different achieved surface states after implantation processing.

Figure 7: Optical micrographs of the surfaces, the wear tracks and measured track widths after 200 cycles with an applied load of 0.5 N.

Figure 8: Measured track widths after 200 cycles with an applied load of 0.5 N.

Figure 9: GIXRD diffraction patterns of non-implanted T-6Al-4V (sample 0) and carbon implanted Ti-6Al-4V (samples 2 and 4).

Figure 10: Raman spectra for all test samples according table 1 showing the crystallinity state of the different surface and implantation conditions.

Figure 11: XPS depth profiling of the C 1s (left) and Ti 2p (right) excitation for sample 5.

Figure 12: Raman spectra of sample 5 for: (a) just after carbon implantation, (b) after a 200 cycles tribology test, (c) after the friction coefficient reaches the value of the non-implanted: 0.6; and (d) for a non-implanted sample (according sample 0)

Highlights

- Development of a new method for surface modifications
- Study of surface properties enhancement by carbon ion irradiation
- Tribological property of titanium alloy Ti-6AL-4V is improved due to the presence of a graphitic carbon layer

Graphical Abstract (for review)

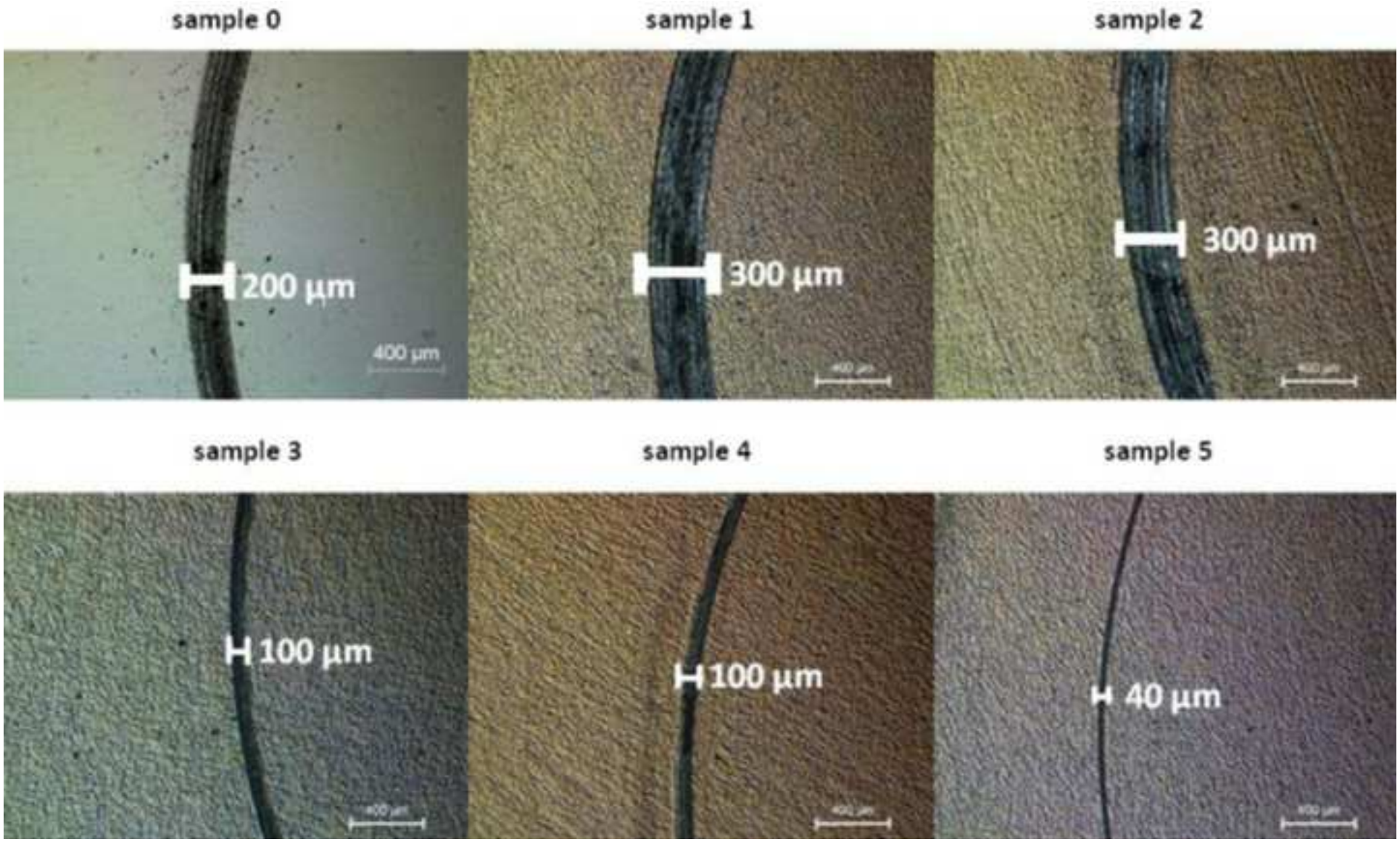

Fig1

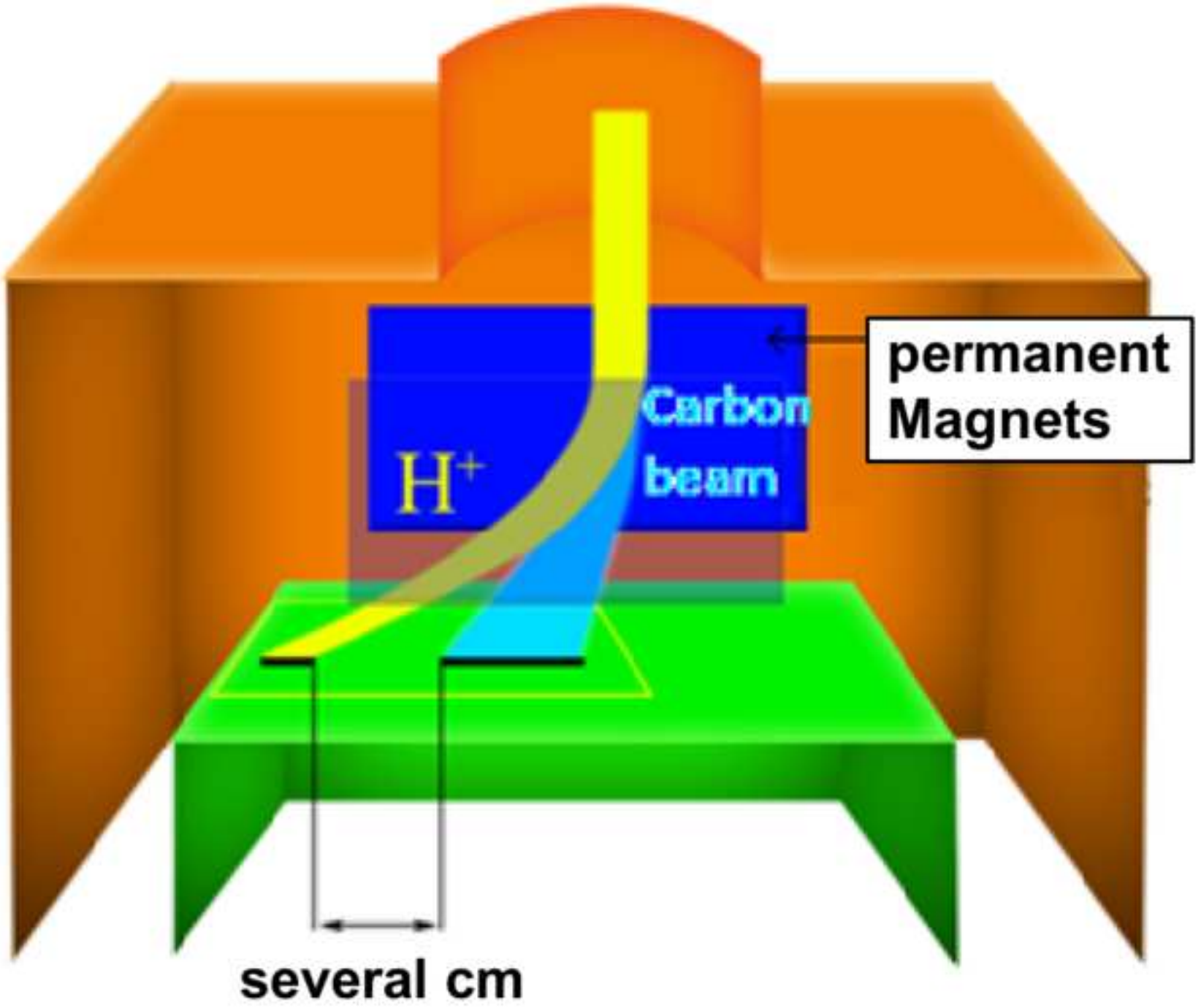

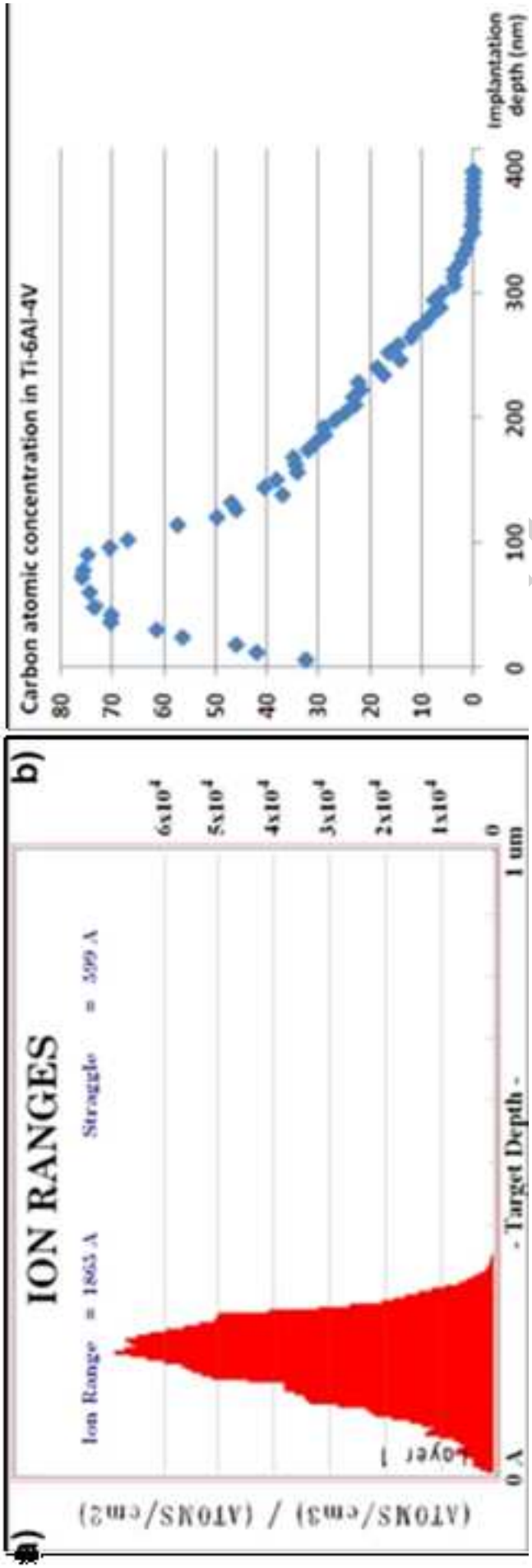

Fig2

Fig3

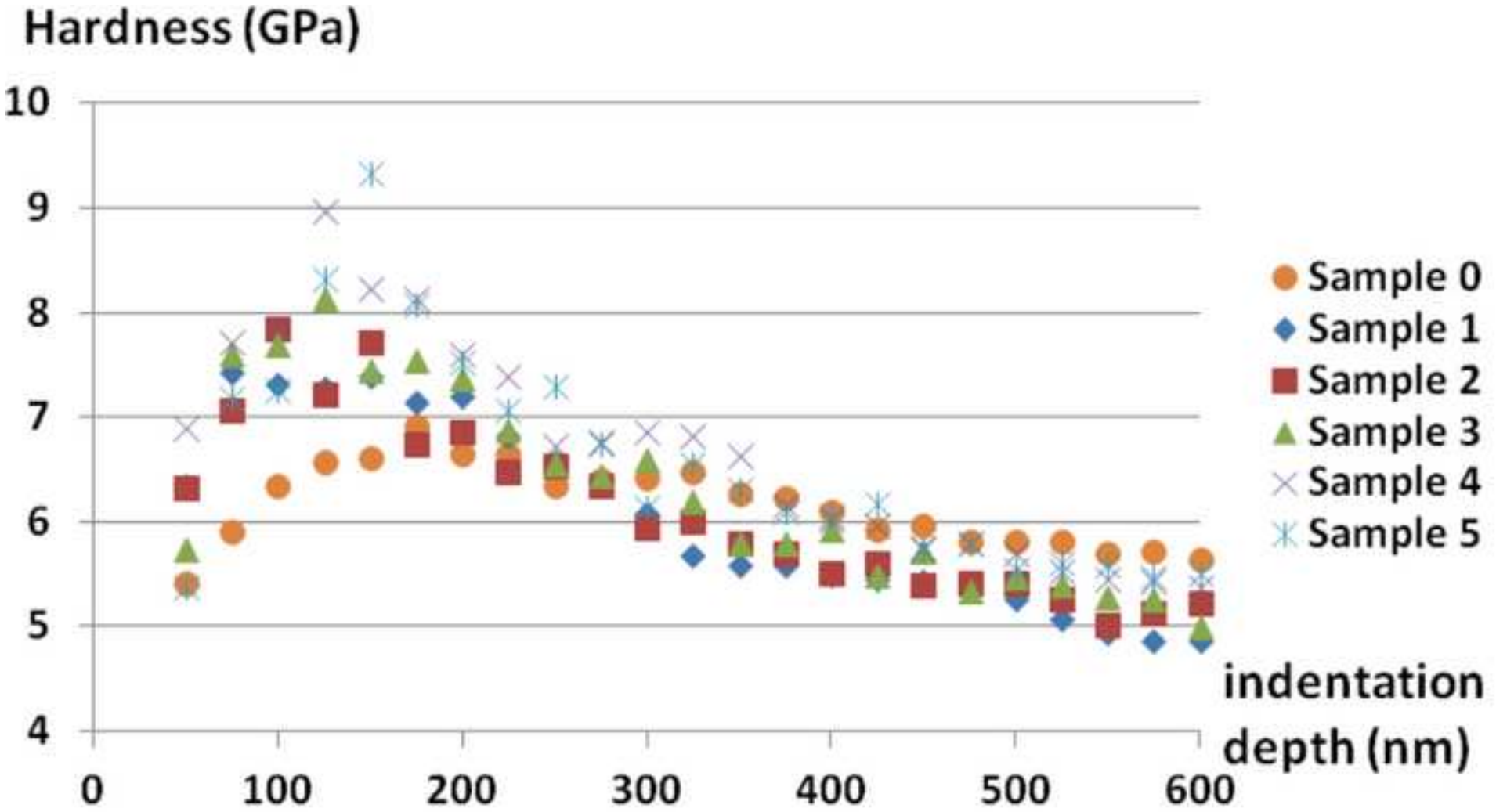

Fig4

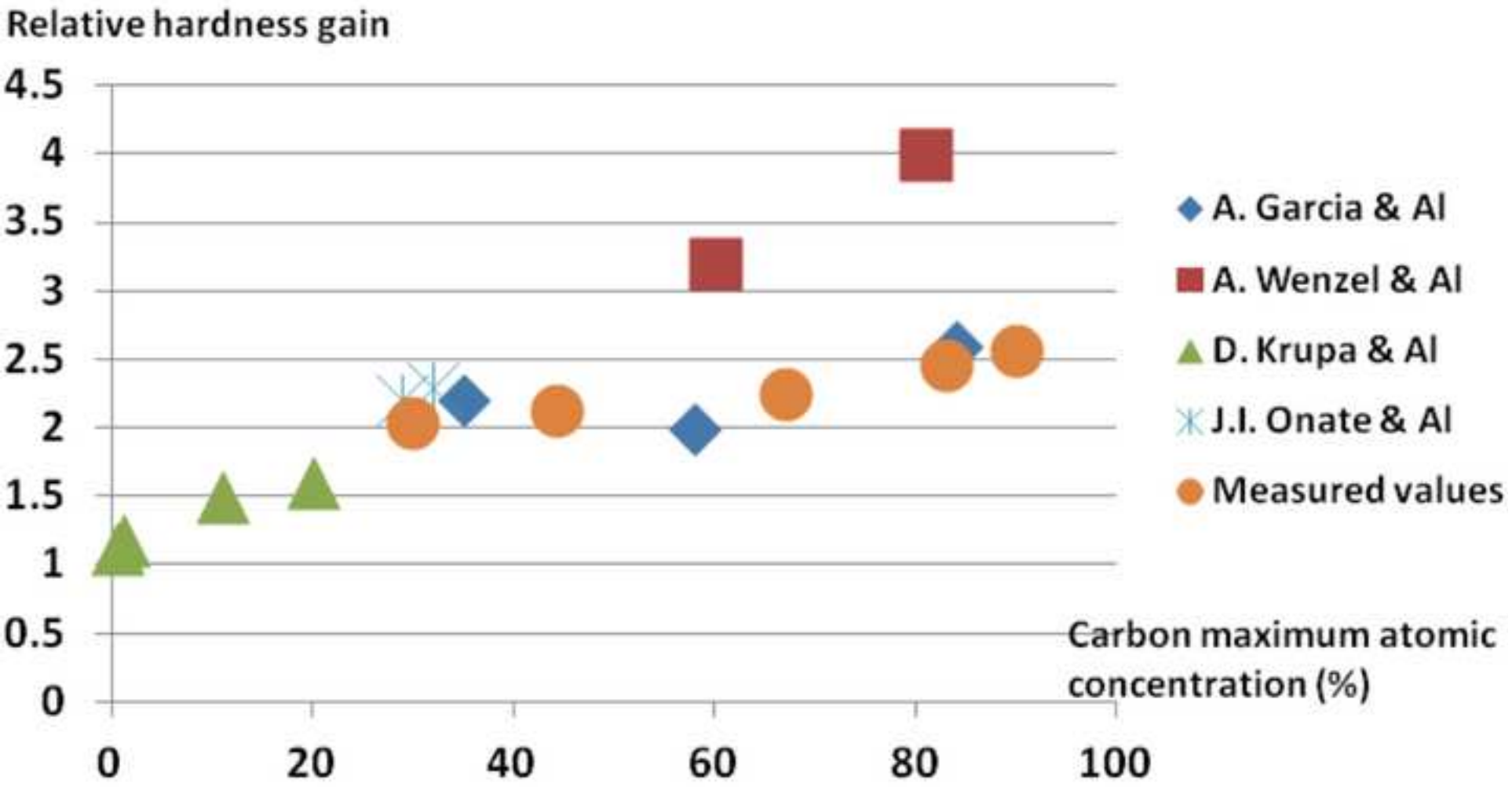

Fig5

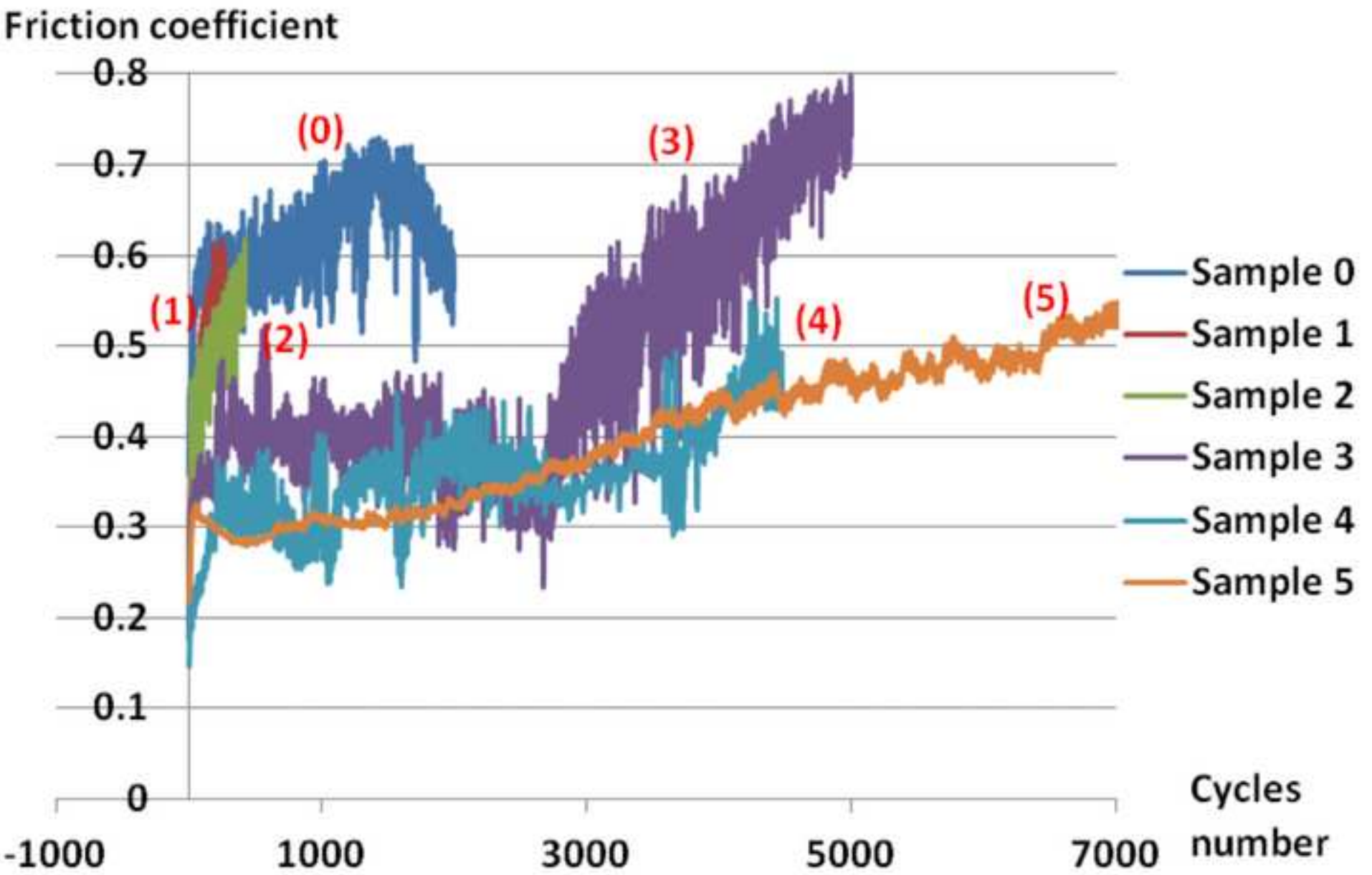

Fig6

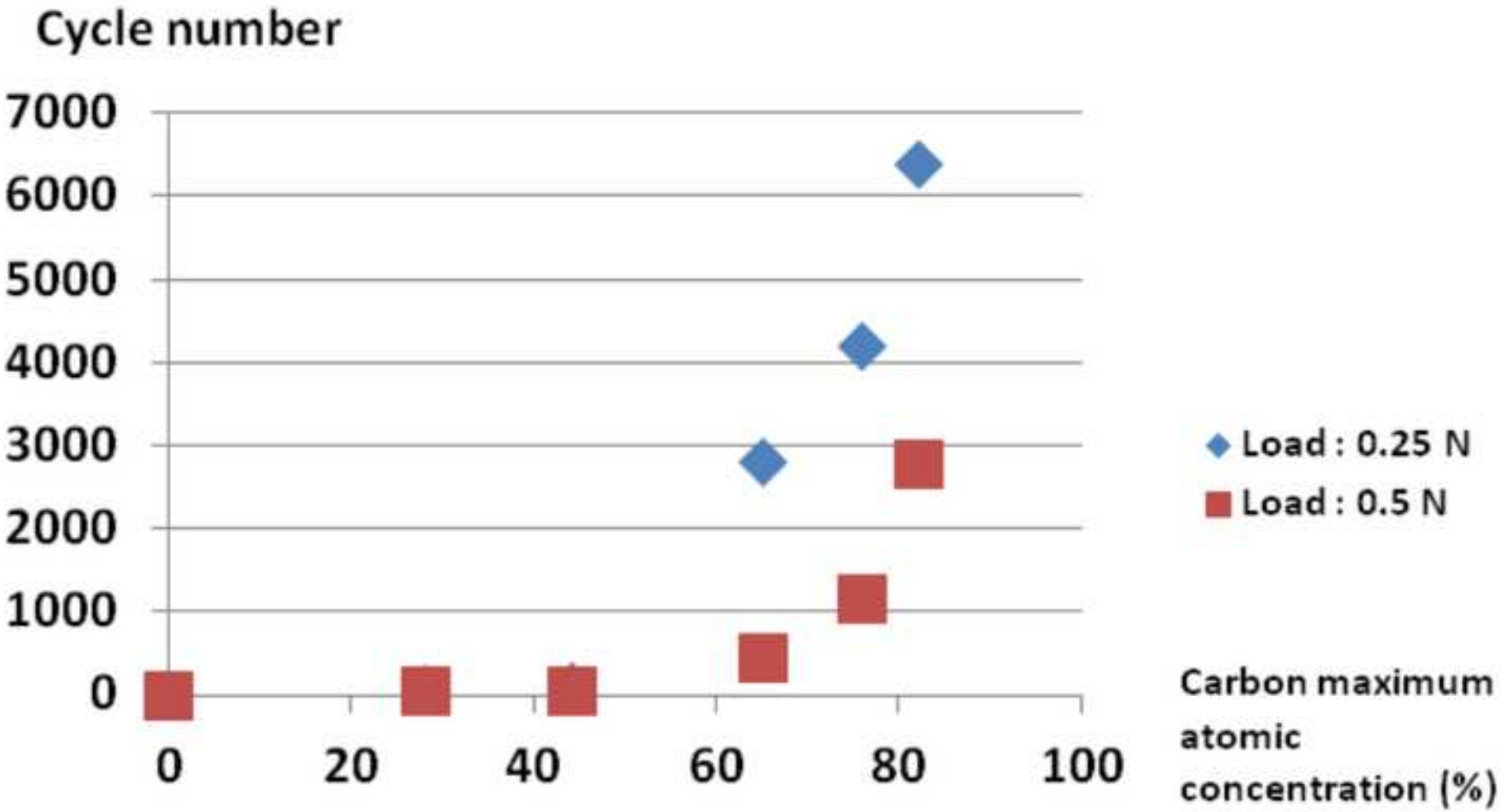

Fig7

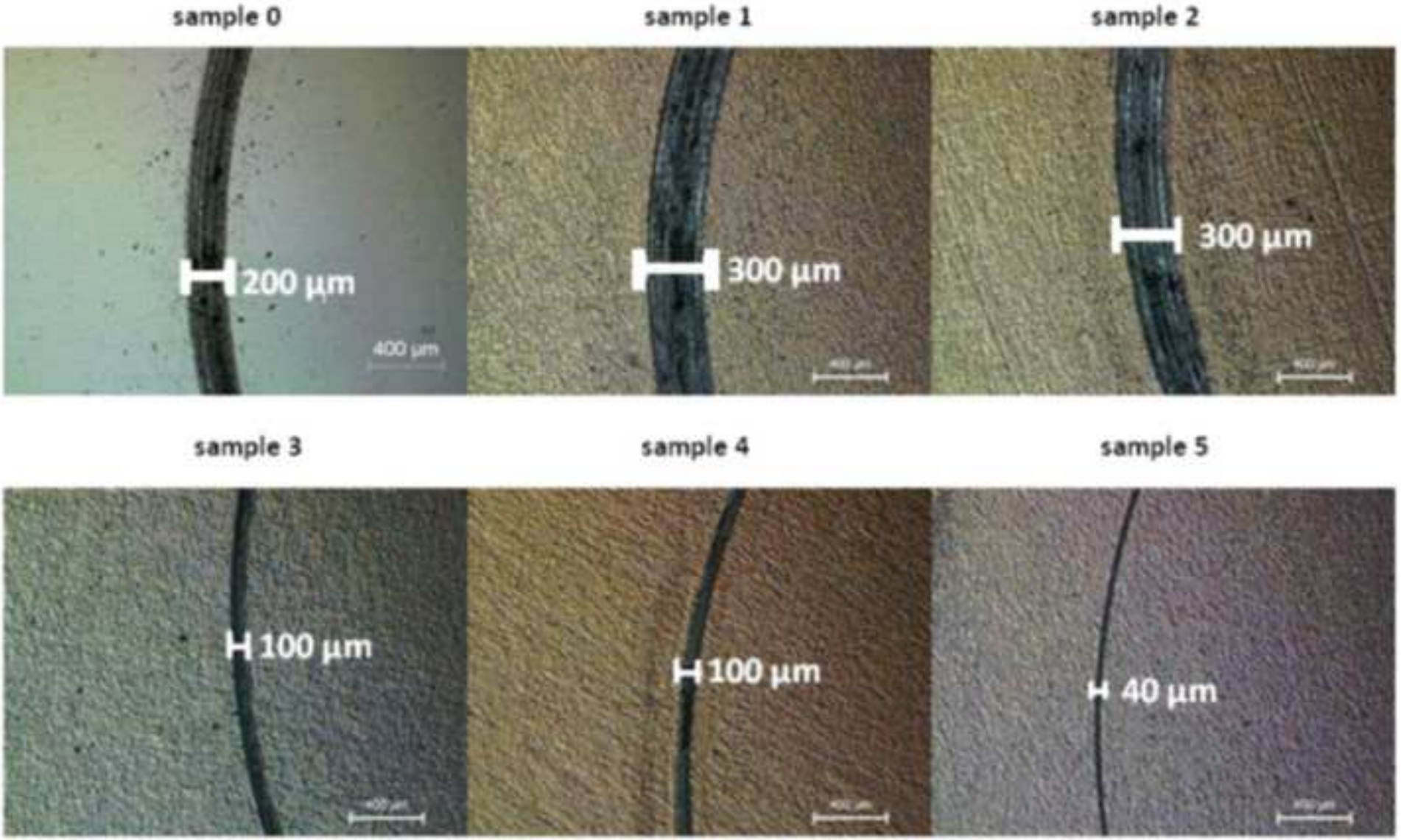

Fig8

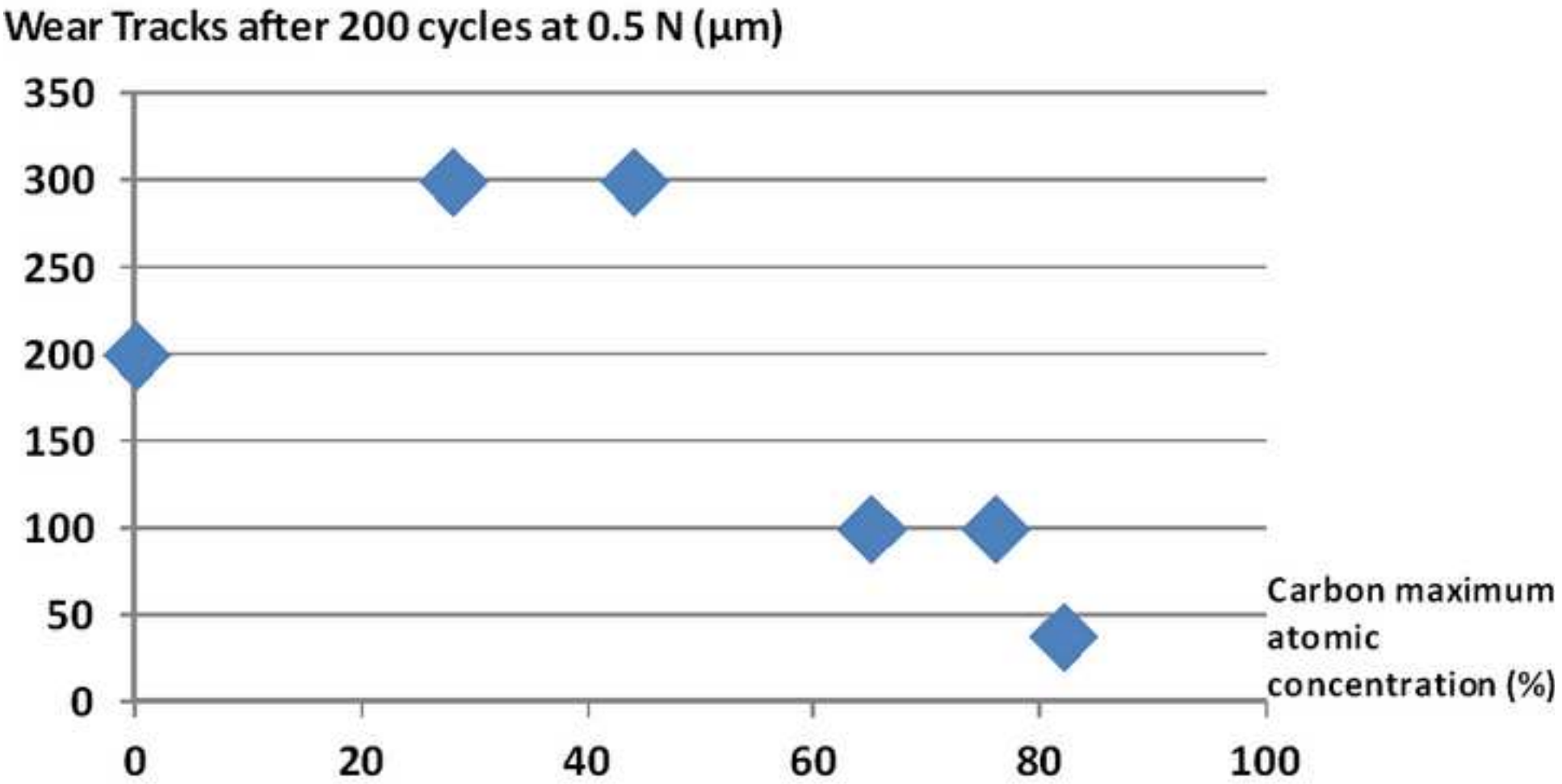

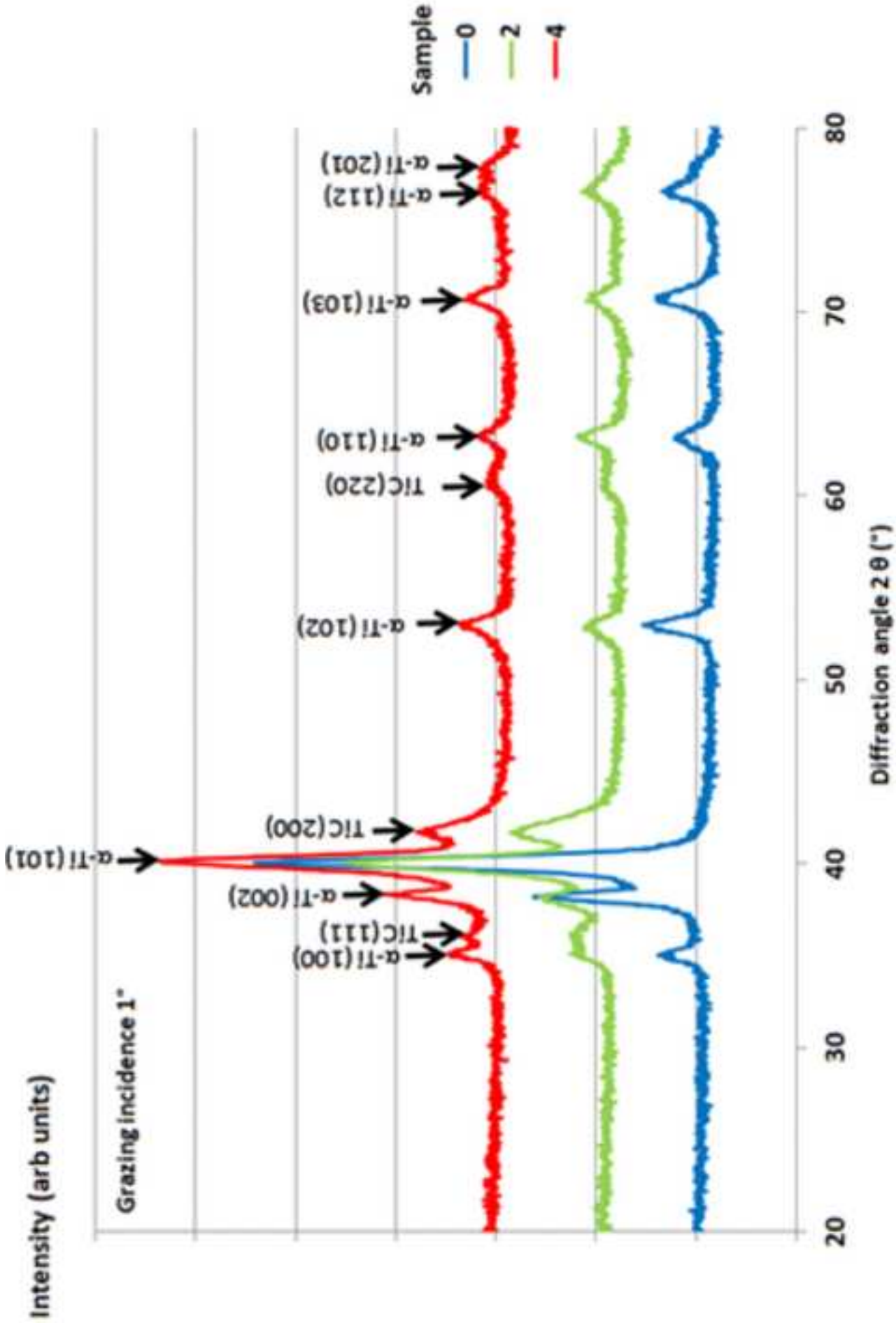
Sample
0
2
4
α-Ti(201)
α-Ti(112)
α-Ti(103)
α-Ti(110)
TiC(220)
α-Ti(102)
TiC(200)
α-Ti(101)
α-Ti(002)
TiC(111)
α-Ti(100)
Grazing incidence 1°
Intensity (arb units)
20
30
40
50
60
70
80
Diffraction angle 2θ (°)

Fig9

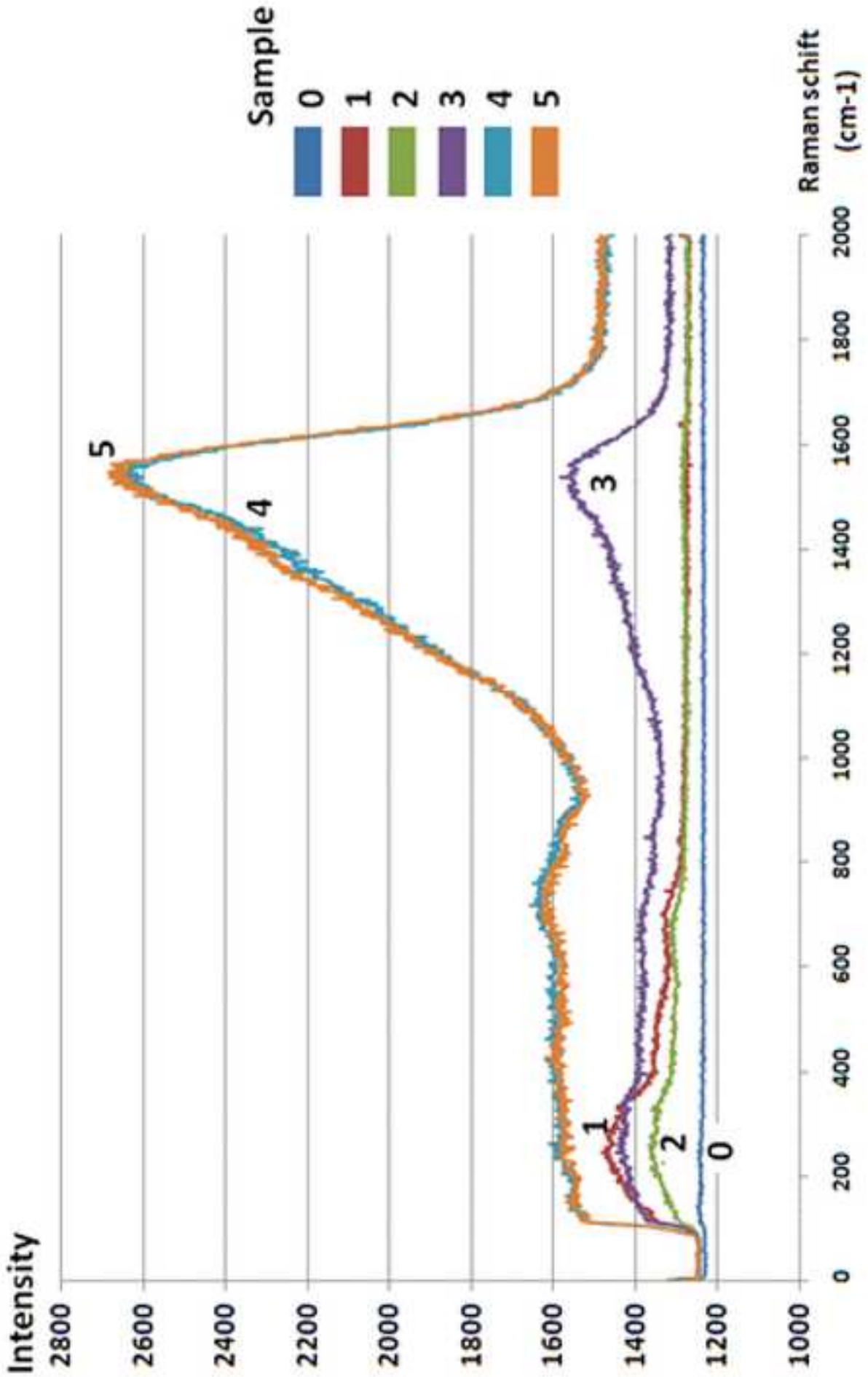

Fig10

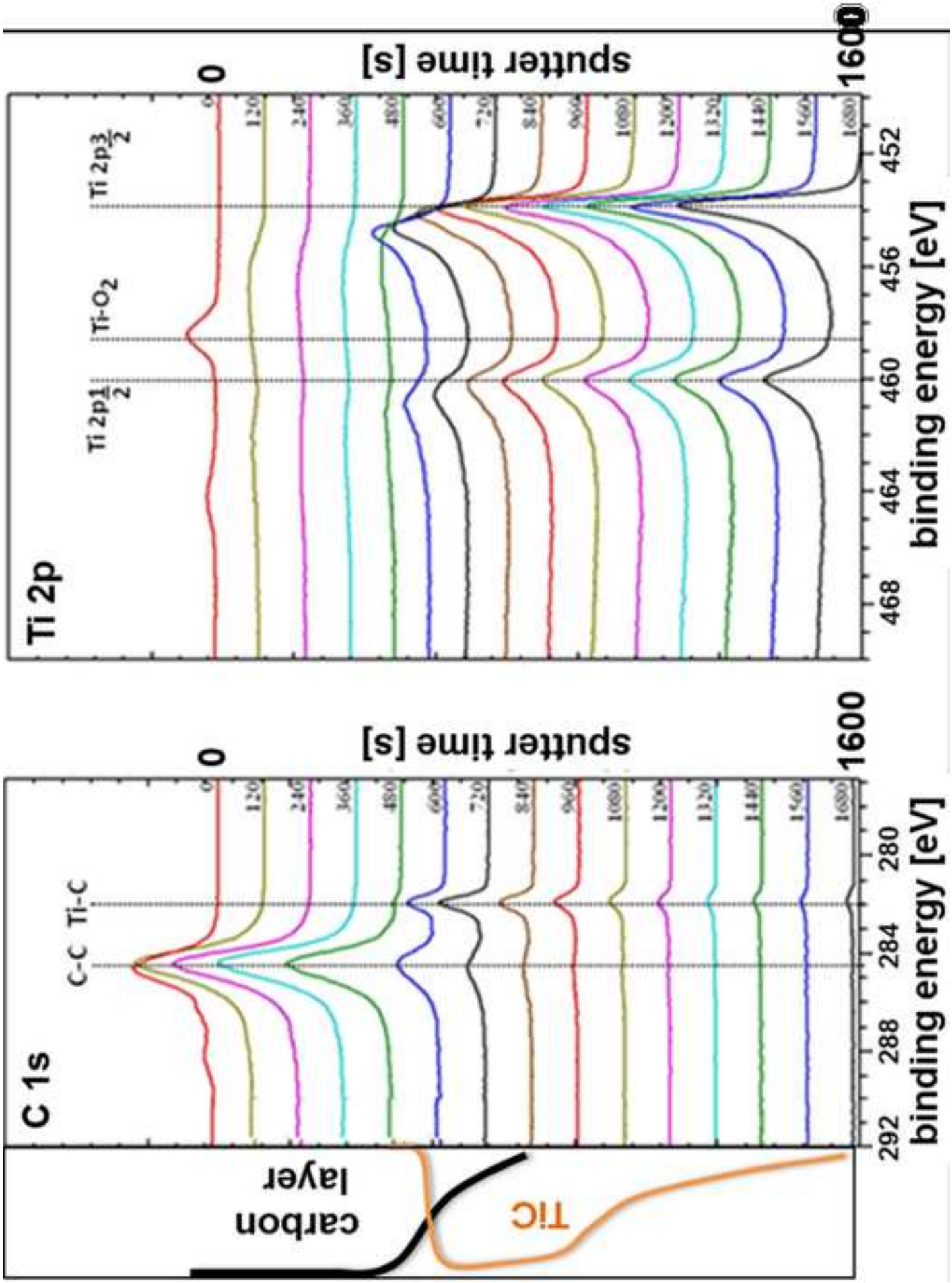
Ti 2p
Ti 2p3/2
Ti-O2
Ti 2p1/2
sputter time [s]
0
1600
binding energy [eV]
452
456
460
464
468
C 1s
C-C
Ti-C
280
284
288
292
carbon layer
TiC

Fig11

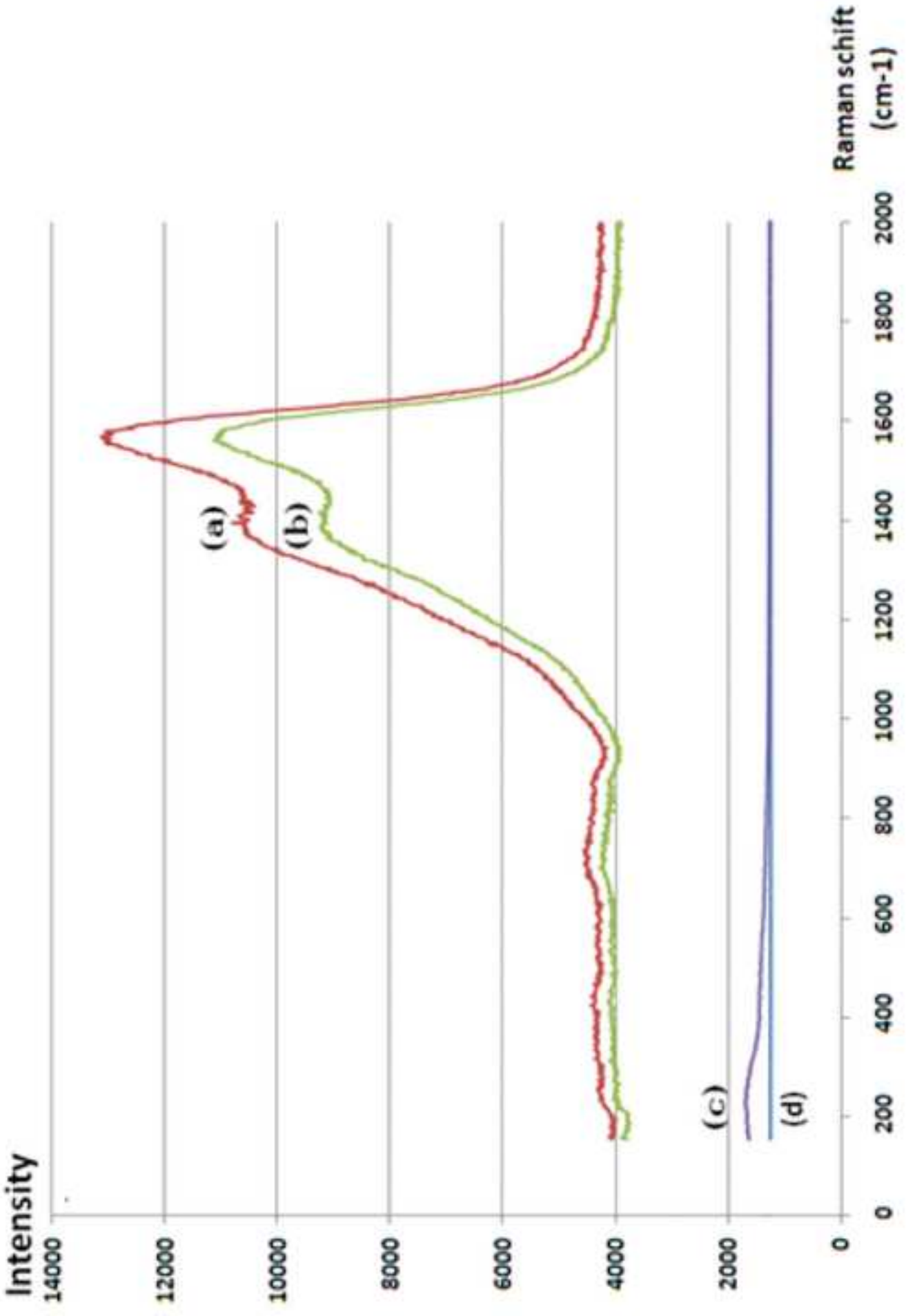
Intensity
14000
12000
10000
8000
6000
4000
2000
0
(a)
(b)
(c)
(d)
0
200
400
600
800
1000
1200
1400
1600
1800
2000
Raman schift
(cm-1)

Fig12